Turk Neurosurg, 2024
**DOI:** 10.5137/1019-5149.JTN.46170-23.2

*Original Investigation*

Stereotactic and Functional

Received: 18.12.2023
Accepted: 24.04.2024

Published Online: 30.12.2024

# Assessing the Potential of Transorbital and Supraorbital Approaches for Stereotactic Surgery: An Anatomical Feasibility Study

Berkhan GENC[1], Nazlı CAKICI OKSUZ[2], Naci Emre AKSEHIRLI[3], Bahar TEKIN[4], Bayram Ufuk SAKUL[4], Mehmet TONGE[3]

[1]Maastricht University, Department of Neurosurgery, Maastricht, Netherlands
[2]Bayrampasa Kolan Hospital, Department of Neurosurgery, Istanbul, Türkiye
[3]Istanbul Medipol University, Department of Neurosurgery, Istanbul, Türkiye
[4]Istanbul Medipol University, Department of Anatomy, Istanbul, Türkiye

**Corresponding author:** Berkhan GENC ✉ berkhan.genc@hotmail.com

## ABSTRACT

**AIM:** To evaluate the supraorbital and transorbital approaches as alternative entry sites and trajectories targeting the nucleus accumbens (NAc), subcallosal cingulate gyrus (SCG), and lateral hypothalamic area (LHA), in cadavers and surgical planning station.

**MATERIAL and METHODS:** The three-dimensional relationship of the identified trajectories within the anterior and middle cranial fossae as well as the stereotactically targeted NAc, SCG, and LHA, were demonstrated through dissection studies conducted in cadavers. To validate the accuracy of the measurements from the cadaver, trajectory planning was replicated using radiological imaging of patients without a space-occupying lesion who underwent gamma knife surgery. These measurements were compared with those from cadavers.

**RESULTS:** The transorbital and supraorbital trajectories did not pass through the lateral ventricles and they can be used for subventricular targets. Additionally, the NAc and LHA can be targeted simultaneously. These trajectories pass along a broader anatomical area within the NAc due to the anatomical orientation of the nucleus.

**CONCLUSION:** These findings suggest that these entry points may offer new opportunities for stimulating different targets in the prefrontal cortex and may serve as an approach for future clinical use.

**KEYWORDS:** Psychosurgery, Stereotactic surgery, Supraorbital, Transorbital, Deep brain stimulation

**NAc:** Nucleus accumbens, **SCG:** Subcallosal cingulate gyrus, **LHA:** Lateral hypothalamic area, **TGN:** Trigeminal neuralgia, **CSF:** cerebrospinal fluid, **AC:** Anterior commissure, **PC:** Posterior commissure

## INTRODUCTION

Transorbital and supraorbital minimaly invasive approaches are used to access intracranial structures in the anterior and middle fossa as well as lesions in the orbit and adjacent sinuses (17,19).

Although the supraorbital approach was originally defined for skull base lesions, recent advancements in microscopic and endoscopic techniques have enabled access to deep-seated lesions and neurovascular structures (2,5,12,17). Growing interest in minimally invasive approaches and advancements in neuroendoscopy popularized the transorbital route for certain

Berkhan GENC : 0000-0001-9578-6584
Nazlı CAKICI OKSUZ : 0000-0003-1480-6235
Naci Emre AKSEHIRLI : 0000-0002-6472-0707
Bahar TEKIN : 0000-0002-2522-8090
Bayram Ufuk SAKUL : 0000-0002-5539-2342
Mehmet TONGE : 0000-0002-0106-9363

intracranial pathologies because it is safer and less traumatic than the traditional transcranial approaches. Furthermore, these transorbital and supraorbital approaches reduce the cosmetic and morbidity-related effects of brain retraction caused by traditional approaches. Although these methods are still being studied endoscopically, their stereotactic benefits and limits have not been extensively discussed yet (6,25).

Currently, the transfrontal lobar trajectory is commonly used in deep brain stimulation (DBS) surgery for neuromodulation. The available technology requires a convexity-entry stereotactic intervention due to the cable-shaped electrodes and their extensions as well as the subcutaneously implantable battery. Although it is possible to access from different regions of the convexity (frontal, parietal, temporal and occipital), the frontal region located in front of the hairline is not preferred in stereotactic procedures for cosmetic reasons. Furthermore, the variable anatomy of frontal sinuses often makes planning stereotactic interventions via the frontal region more challenging. Thus, approaches such as the transorbital and supraorbital approaches, with an incision within the eyebrow region, can be considered due to its cosmetic and anatomical advantages. Recent technological developments suggest that, in the near future, stimulators that are independent of cables and battery, smaller, and only the size of the anatomical target, will be available. Thus, the absence of other system components may enable more options in terms of stereotactic safety and comfortable approaches.

The limitations of traditional stereotactic trajectories, especially those used in the treatment of psychosurgical targets (e.g., subgenual cingulate cortex [SCG] and nucleus accumbens [NAc]) and hypothalamic targets (e.g., for the treatment of obesity, aggression, and hamartomas) have been discussed in literature (10,28,30,35).

In this study, we aimed to evaluate the minimally invasive transorbital and supraorbital approaches from a stereotactic perspective and identify new trajectories. The three-dimensional relationship of the identified trajectories within the anterior and middle cranial fossa as well as the stereotactically targeted NAc, SCG, and lateral hypothalamic area (LHA) were demonstrated via cadaveric dissection studies. Furthermore, to demonstrate the applicability of these trajectories, anatomical measurements obtained from cadavers were compared with those obtained on stereotactic planning images of patients with primary trigeminal neuralgia (TGN) and without intracranial space-occupying lesions who underwent gamma knife radiosurgery. Herein, we aimed to present and discuss novel transorbital and supraorbital stereotactic trajectories for SCG, NAc and LHA anatomically and radiologically.

## MATERIAL and METHODS

The study was conducted in the Anatomy Laboratory of Istanbul Medipol University after obtaining approval from the local ethics committee (No: 04.02.2021-156).

The study design was examined by the Non-Interventional Clinical Research Ethics Committee of Istanbul Medipol University on 04.02.2021, and it was unanimously decided that the research is ethically and scientifically appropriate after the rationale, purpose, approach and methods of the research were considered.

Frame-based stereotactic transorbital and supraorbital approaches were demonstrated on cadaveric heads following fixation, stereotactic imaging, and stereotactic planning. All three targets (SCG, NAc and LHA) were reached by insertion of a stereotactic biopsy probe along the planned trajectory. Subsequently, the anatomical layers from entry point to target were dissected under the guidance of a surgical microscope. The dissection procedure was meticulously documented using microscopic and endoscopic video as well as direct photographs. To augment the sample size and demonstrate the applicability of the cadaveric measurements, radiological images of 20 patients (40 hemispheres) with primary TGN and without an intracranial space-occupying pathology, who had previously undergone gamma knife radiosurgery were included in the study (TGN group). The transorbital and supraorbital trajectories for the aforementioned targets were re-planned using magnetic resonance imaging (MRI) obtained for radiosurgery planning and surgical planning stations used for DBS surgery. The stereotactic parameters of the approaches were statistically analyzed.

### Cadaveric Fixation Technique

Four, unfixed, fresh-frozen, cadaver heads were used for stereotactic application and anatomical dissection. Two of the specimens were females, and the other two were males. All the cadavers were adults. The cadaver heads used in the study had been decapitated at the C7–T1 level. To maintain consistency in the specimens and minimize potential confounding factors that could impact the validity of the results, only the heads of cadavers that did not exhibit any fractures, which could impair bone integrity, or have a prior history of cranial surgeries were included in the study.

To ensure vascular visualization during the dissection, the colored silicone injection technique was used (31). Additionally, using the right Kocher's point, an external ventricular drainage catheter was inserted into the lateral ventricles of each cadaver head, and possible pathologies within the ventricular system were assessed. Approximately 20–30 cc of cerebrospinal fluid (CSF) was drained from the ventricular system and replaced with an equal volume of the fixation solution.

Each specimen was stored at 10°C in containers filled with fixation fluid for at least three weeks following complete fixation, until they were dissected.

### Stereotactic Planning & Surgical Procedure

Stereotactic coordinates were acquired using the Leksell stereotactic system (Elekta Instruments, Stockholm, Sweden) for a total of 18 bilateral interventions on three fixed cadavers. One cadaver was used for the pilot study to assess the fixation technique. A total of 18 stereotactic targets (bilateral SCG, NAc and LHA) were studied using stereotactic supraorbital and superior transorbital approaches.

A Leksell G-frame was mounted on the cadaveric head, at a rotation of 45° in the sagittal plane and 3 cm superior to the

glabella, to achieve access to both orbits. Furthermore, the front part of the frame was replaced with a flat piece designed to allow for a full lateral approach (Figure 1). Subsequently, T1- and T2-weighted MRI and computerized tomography (CT), with a slice thickness of 1 mm, were performed (Figure 2).

The TGN group comprised of 20 stereotactic MRIs of patients with primary TGN. Stereotactic coordinates were calculated using Elements (Brainlab, Munich, Germany), StealthStation (Medtronic, Dublin, Ireland), and 3D slicer (9). Indirect stereotactic coordinates for SCG, NAc and LHA were established using the "Atlas of the Human Brain" (22). Stereotactic trajectories were planned in line with accepted stereotactic principles. Trajectories trespassing vascular structures, sulci, ventricles, and frontal sinuses were avoided. The x, y, and z coordinates and biplanar angles of the approach (arc and ring angles) for each individual target were recorded and applied within the Leksell stereotactic arc system.

In the supraorbital approach, a 2-cm eyebrow incision was made, and the supraorbital ridge and margin were exposed subperiosteally. The medial and lateral boundaries of the craniectomy, which would be used as the stereotactic entry point, were the supraorbital notch and eyebrow tail, respectively. Care was taken to stay lateral to the frontal sinus to avoid passing through it during the craniectomy (Figure 3).

In the transorbital approach, an incision was made along the inferior margin of the eyebrow. Subsequently, subperiosteal dissection was performed to expose the supraorbital margin and orbital roof. The medial and lateral limits of the craniotomy were the supraorbital notch and lacrimal gland, respectively (Figures 4,5).

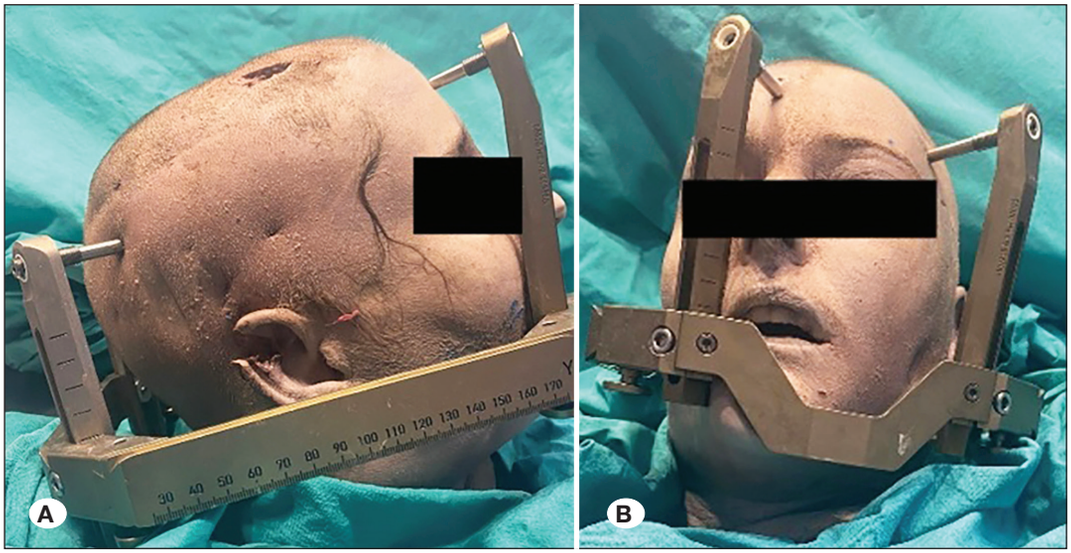


**Figure 1:** Placement of the Leksell head frame. **A)** Front view and **B)** side view.

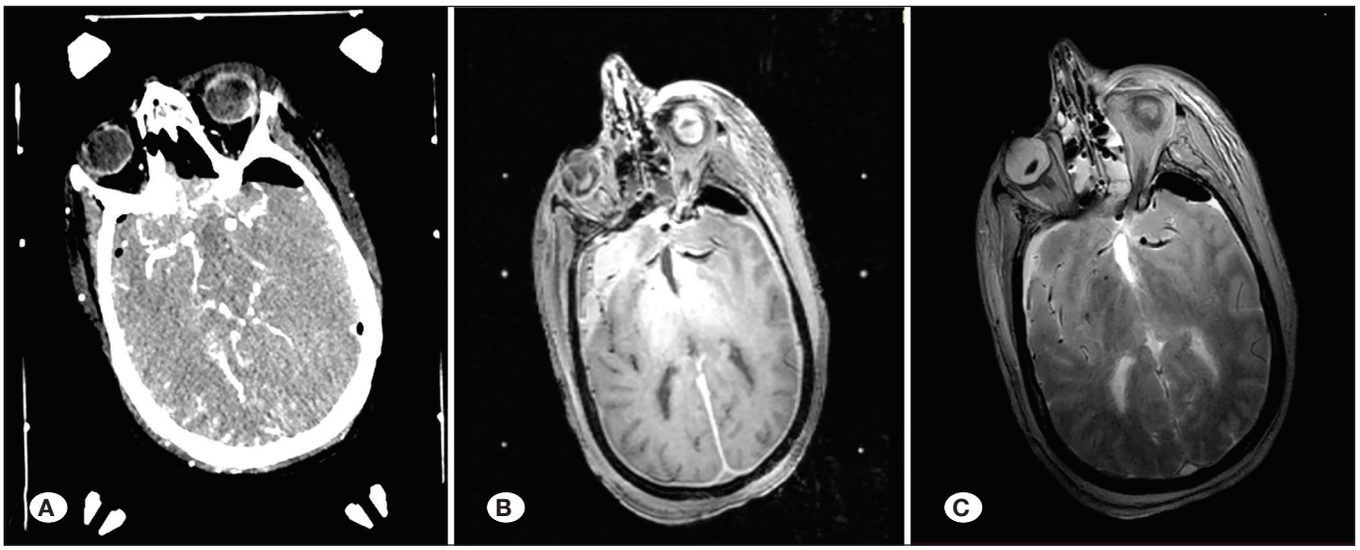


**Figure 2:** Radiological images of the cadaver heads. **A)** computed tomography, **B)** T1-weighted magnetic resonance imaging, and **C)** T2-weighted magnetic resonance imaging.

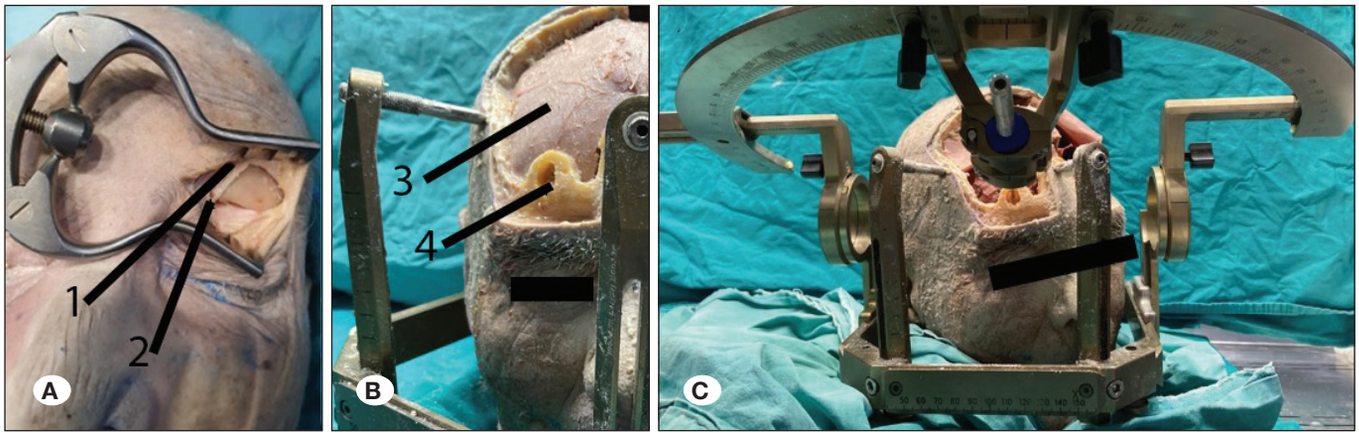


**Figure 3:** Supraorbital approach. **A)** 1) Supraorbital nerve and 2) supraorbital notch. **B)** 3) Dura mater and 4) Burr hole for the entry. **C)** Stereotactic biopsy system inserted view.


**Figure 4:** Eyebrow incision and subperiosteal dissection. **1)** Supraorbital margin, **2)** transorbital approach, **3)** orbital roof, and **4)** supraorbital nerve.

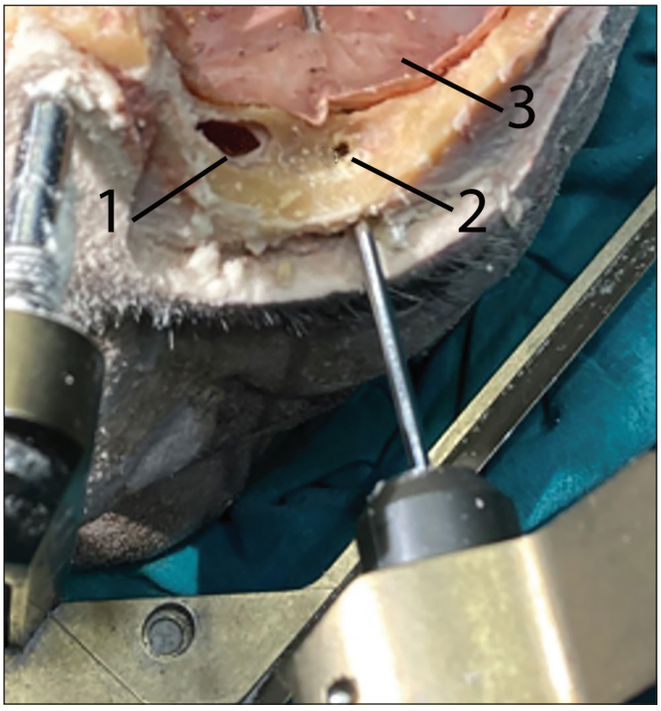


**Figure 5:** Transorbital approach. **1)** Frontal sinus, **2)** periorbita, and **3)** supraorbital dura.

Stereotactic biopsy probes were inserted into the targets through the burr hole. Once the targets on the right side were marked, the arc system was repositioned in the anterior-posterior orientation to enable a full lateral approach on the left side. The x and y coordinates were adjusted as x = y1 and y = x1, and the targets for the left side were marked based on the x1 and y1 coordinates. After marking the targets, a frontal craniotomy was performed, and 1-cm thick coronal sections were collected using sharp dissection (Figure 6).

### Stereotactic Targets

The stereotactic coordinates of the NAc were indirectly calculated using the "Atlas of the Human Brain" (22); the most distal anatomical target was aligned with the most distal contact of the electrode. The indirect atlas coordinates were modified using image processing programs and MRIs (Figure 7). The NAc location was confirmed in coronal T1-weighted images by visualizing its position inferior to the lateral ventricle and inferomedial to the caudate nucleus, internal capsule, and putamen. The vertical limb of Broca's diagonal band and the olfactory tubercle were identified as the medial and ventral target boundaries, respectively (Figure 8) (33,34).

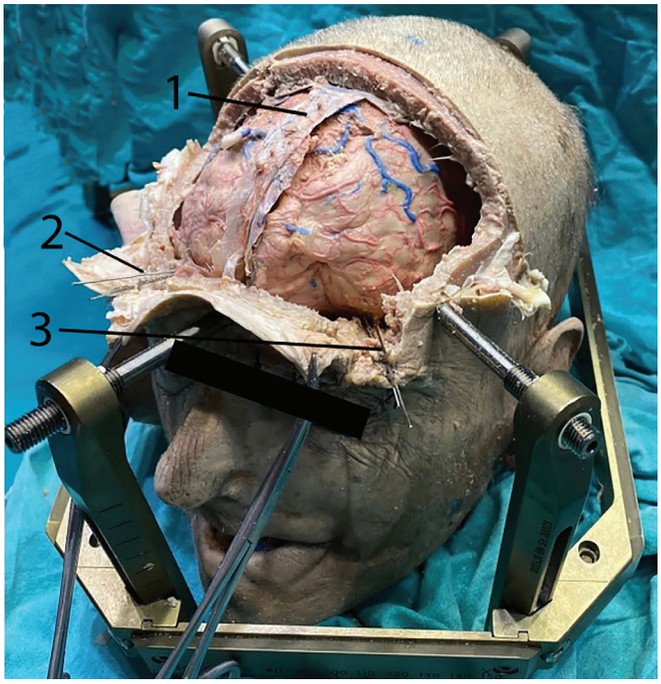


**Figure 6:** Excision of the frontal bone. **1)** Sagittal sinus, **2)** wires placed supraorbital to the target, and **3)** wires placed transorbital to the target.

Coordinates for the ventral region of the subcallosal cingulate gyrus were obtained using the Atlas of the Human Brain and the targets studied in the treatment of treatment-resistant depression (Figures 9,10) (14,22).

The LHA, which has been studied as a target in treatment-resistant obesity, was chosen as the hypothalamic target. According to the planning images, the target would be approximately 6.5 mm lateral and 3 mm below the intercommissural line as well as 4.5 mm posterior to the anterior commissure (AC) (Figures 11,12) (35).

## RESULTS

Besides the three cadaveric specimens, eleven female and nine male patients with a diagnosis of primary TGN and without an intracranial space-occupying pathology, were included. The mean age of the patients in the study group was 53.4 ± 18.7 years (range: 24–96 years).

We assessed the trajectories targeting NAc, SCG, and LHA via different entry points in cadavers. For NAc, the mean trajectory length via the transorbital, supraorbital, and Kocher's approaches was 63.31 ± 3.20 mm (range: 55.28–71.17), 67.93 ± 2.43 mm (range: 61.77–75.96), and 76.94 ± 4.545 mm (range: 71.78–84.05), respectively. For SCG, the mean trajectory length via the transorbital, supraorbital, and Kocher's approaches was 54.06 ± 1.88 mm (range: 49.23–60.31),

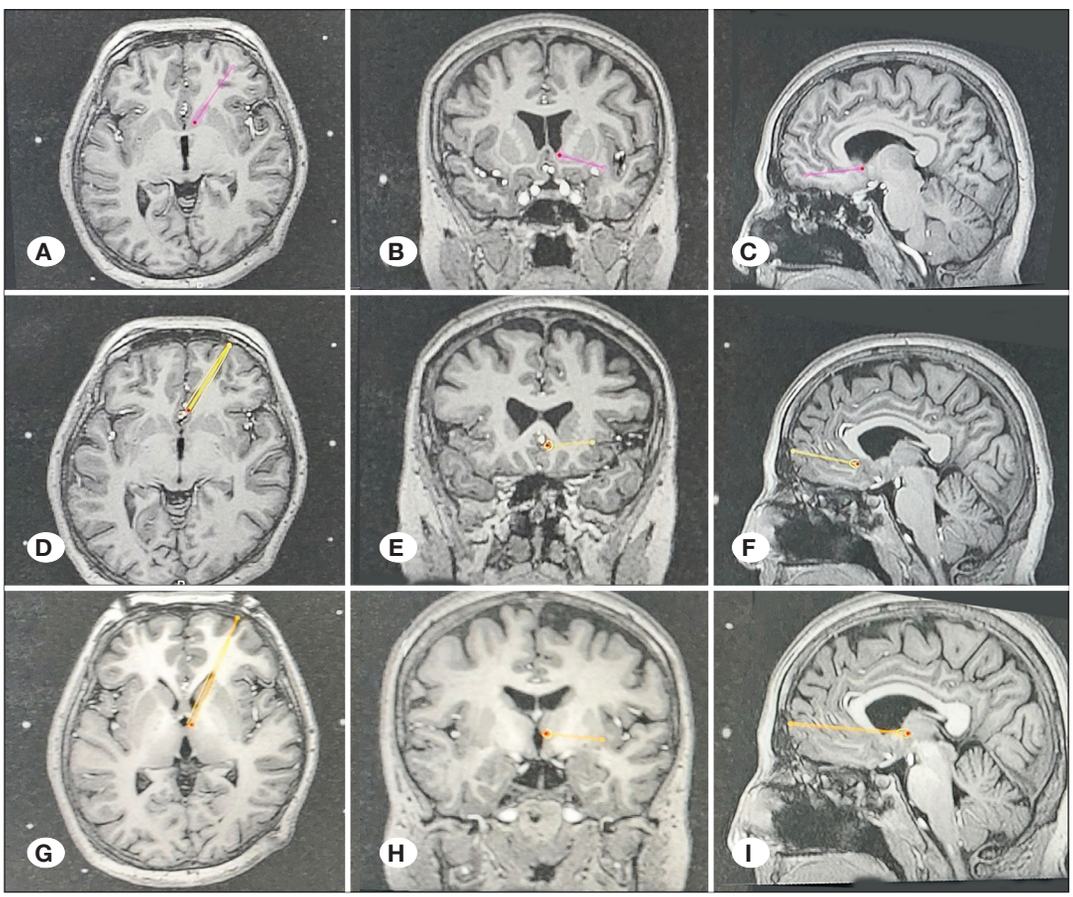


**Figure 7:** Planned trajectories of the targets. Trajectory to the nucleus accumbens in the **A)** axial plane, **B)** coronal plane, and **C)** sagittal planes. Trajectory to the subgenual cingulate in the **D)** axial plane, **E)** coronal plane, and **F)** sagittal planes. Trajectory to the lateral hypothalamic area in the **G)** axial plane, **H)** coronal plane, and **I)** sagittal planes.

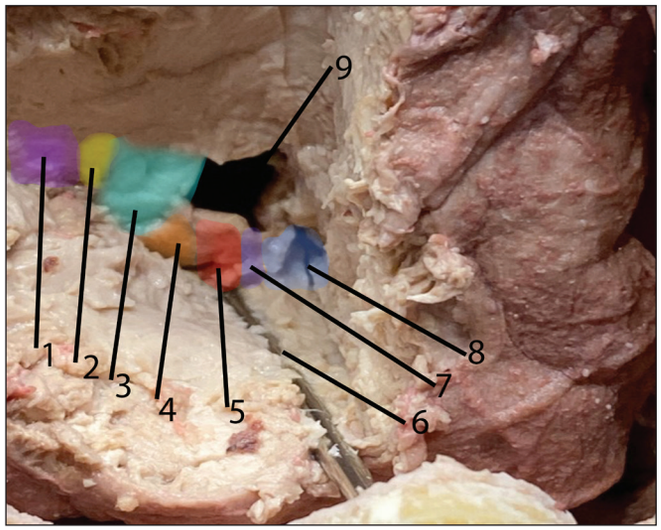


**Figure 8:** Dissection of the trajectory to the nucleus accumbens via the supraorbital approach. **1.** Putamen, **2.** internal capsule, **3.** caudate nucleus, **4**. lateral nucleus accumbens, **5.** Medial Nucleus Accumbens, **6.** stereotactic trace, **7.** The diagonal band of Broca, **8.** Brodmann area 25 and **9.** lateral ventricle.

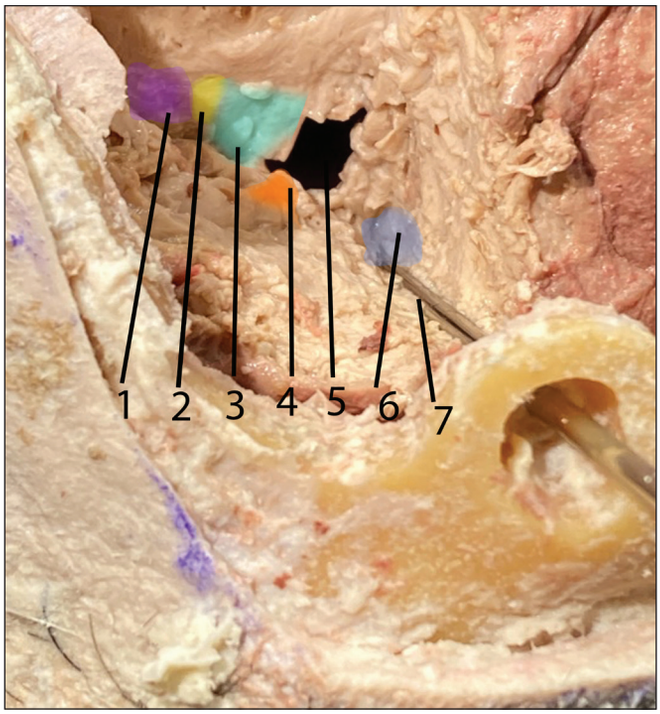


**Figure 9:** Dissection of the trajectory to the subcallosal cingulate gyrus via the supraorbital approach. **1.** Putamen, **2.** internal capsule, **3.** caudate nucleus, **4.** nucleus accumbens, **5.** lateral ventricle, **6.** subcallosal cingulate gyrus and **7.** stereotactic trajectory (Right supraorbital entry).

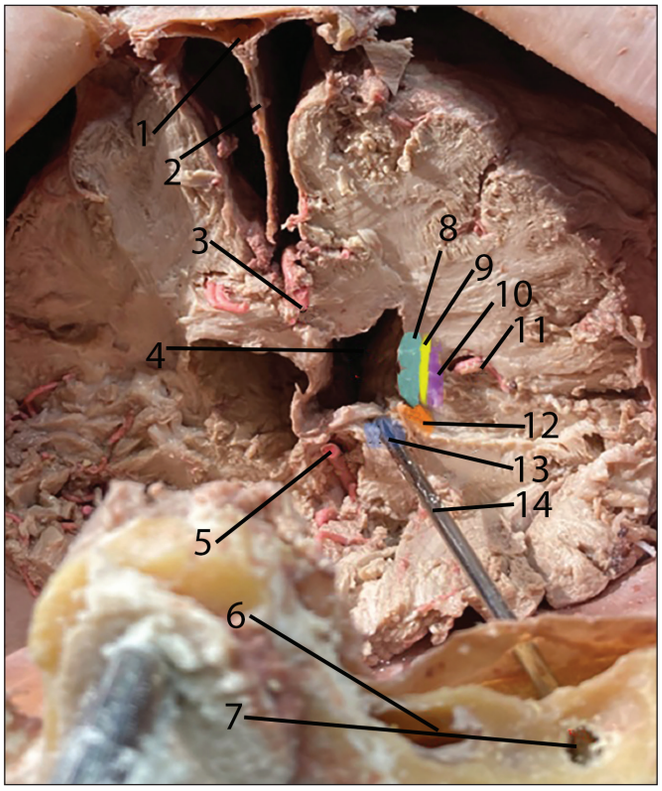


**Figure 10:** Dissection of the trajectory to the subcollosal cingulate gyrus via the transorbital approach**. 1.** Sagittal sinus, **2.** falx cerebri, **3.** pericollosal artery, **4.** lateral ventricle, **5.** basillary artery, **6.** frontal sinus, **7.** orbit, **8.** caudate nucleus, **9.** internal capsule, **10.** Putamen, **12.** nucleus Accumbens, **11.** sylvian fissure, **13**. subcallosal cingulate gyrus and **14**. stereotactic trajectory (left transorbital entry).

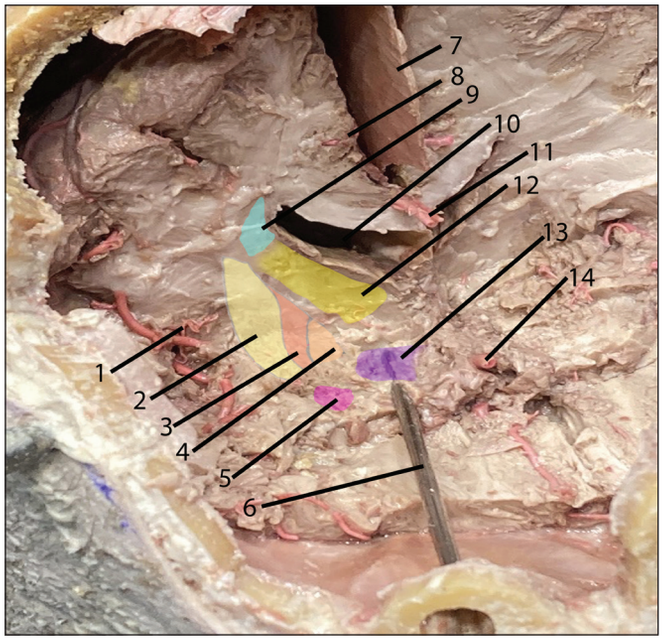


**Figure 11:** Dissection of the trajectory to the lateral hypothalamic area via the supraorbital approach. **1.** Sylvian fissure, **2.** putamen, **3.** external globus pallidus, **4.** internal globus pallidus, **5.** amygdala**, 6.** stereotactic trace (right suprorbital entrance), **7.** falx, **8.** callosomarginal artery, **9.** caudate nucleus, **10.** lateral ventricle **11**. pericallosal artery, **12.** thalamus, **13.** posterior hypothalamic area, and **14.** basillary artery.

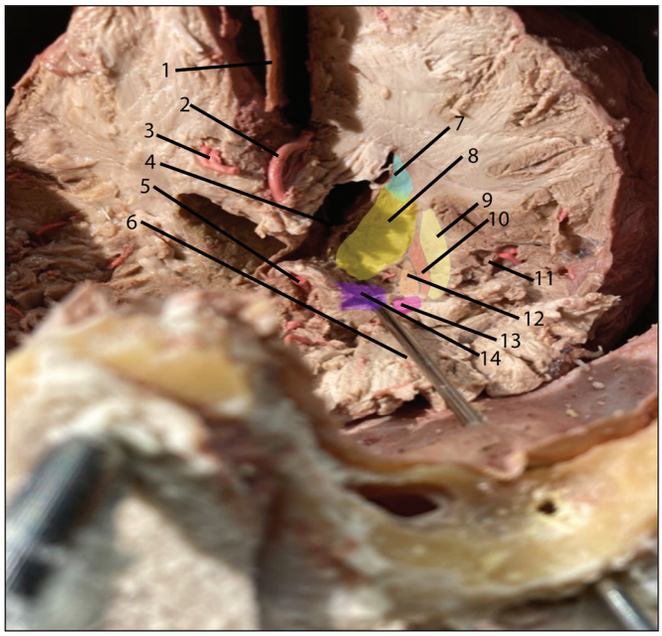


**Figure 12:** Dissection of the trajectory to the lateral hypothalamic area via the transorbital approach. **1.** Falx, **2.** pericallosal artery, **3.** callosomarginal artery, **4.** lateral ventricle, **5.** basillary artery, **6.** stereotactic trajectory (left transorbital entry), **7.** caudate, **8.** thalamus, **9.** putamen, **10.** external globus pallidus, **11.** sylvian fissure, **12**. internal globus pallidus, **13.** Amygdala, and **14.** posterior hypothalamic area.

57.87 ± 1.75 mm (range: 50.35–63), and 74.83 ± 3.12 mm (range: 69.35–79.09), respectively. For LHA, the mean trajectory length via the transorbital, supraorbital, and Kocher's approaches was 77.46 ± 2.43 mm (range: 69.70–82.54), 81.6 ± 2.65 mm (range: 71.18–89.48), and 77.46 ± 7.30 mm (range: 69.87–84.54), respectively.

For targeting the NAc in patients with TGN, the mean trajectory length via the transorbital and supraorbital approaches was 41.99 ± 0.72 mm (range: 31.60–50.40) and 55.30 ± 0.54 mm (range: 50.10–64.70), respectively. For targeting the SCG in patients with TGN, the mean trajectory length via the transorbital and supraorbital approaches was 35.20 ± 4.44 mm (range: 24.90–43.60) and 46.79 ± 0.52 mm (range: 41.60–57.60), respectively. For targeting the LHA in patients with TGN, the mean trajectory length via the transorbital and supraorbital approaches was 54.31 ± 0.75 mm (range: 42.90–65.20) and 67.57 ± 0.64 mm (range: 59.00–75.80), respectively.

In the cadavers, the angles formed by trajectories targeting the NAc, LHA, and SCG, using the anterior commissure, posterior commissure (AC-PC) points and the midline, were measured in the sagittal and axial planes. In the cadavers, the mean angle formed by the trajectories targeting the NAc, SCG, and LHA via the transorbital approach in the sagittal plane was 115.40 ± 4.23° (range: 103.20–129.30), 113.70 ± 4.86° (range: 101.70–130.30), and 118.21 ± 3.71° (range: 104.90–128.60), respectively. The mean angle formed by the trajectories targeting the NAc, SCG, and LHA via the supraorbital approach in the sagittal plain was 94.25 ± 5.66° (range: 75.60–110.00), 91.76 ± 7.59° (range: 77.50–120.70), and 107.03 ± 9.19° (range: 90.00–150.50), respectively.

In the cadavers, the mean angle formed by the trajectories targeting the NAc, SCG, and LHA via the transorbital approach in the axial plane was 8.10 ± 1.46° (range: 2.60–11.50), 9.76 ± 2.20° (range: 0.70–14.70), and 10.93 ± 2.29° (range: 2.80–17.00), respectively. The mean angle formed by the trajectories targeting the NAc, SCG, and LHA via the supraorbital approach in the axial plane was 6.11 ± 1.68° (range: 1.40–11.60), 8.46 ± 1.40° (range: 3.90–12.40), and 5.7833 ± 2.10245° (range: 0.10–13.10), respectively.

The angles formed by the trajectories in the sagittal and axial planes in patients with TGN were measured using the AC-PC points and midline. In patients with TGN, the mean angle formed by the trajectories targeting the NAc, SCG, and LHA via the transorbital approach in the sagittal plane was 110.88 ± 2.00° (range: 103.20–129.30), 102.72 ± 2.90° (range: 11.60–133.20), and 116.89 ± 2.23° (range: 89.30–149.20), respectively. The mean angle formed by the trajectories targeting the NAc, SCG, and LHA via the supraorbital approach in the sagittal plane was 88.07 ± 2.82° (range: 49.60–129.80), 82.44 ± 2.10° (range: 11.60–133.20), and 94.03 ± 2.65° (range: 64.60–133.50), respectively.

In patients with TGN, the mean angle formed by the trajectories targeting NAc, SCG, and LHA via the transorbital approach in the axial plane was 13.31 ± 1.26° (range: 0.3–37.40), 16.92 ± 1.57° (range: 1.30–49.9), and 14.00 ± 1.29° (range: 0.3–39.9), respectively. The mean angle formed by the trajectories targeting the NAc SCG, and LHA via the supraorbital approach in the axial plan was 7.40 ± 1.05° (range: 0.50–24.80), 8.68 ± 1.24° (range: 0.00–38.70), and 6.51 ± 0.89° (range: 0.00–24.10), respectively.

When planning trajectories via the supraorbital approach, the trajectory passed through the right frontal sinus in only one cadaver. In the cases used for radiological measurements, out of a total of 20 cases, the trajectory passed through the frontal sinus in one patient for a right-sided entry, in two patients for a left-sided entry, and in two patients for right- and left-sided entries, resulting in a total of 5 trajectories passing through the frontal sinus (Figure 13). The trajectories used in the transorbital approach do not pass through the frontal sinus. Additionally, using the transorbital approach, the LHA and NAc can be targeted simultaneously (Figure 14).

There was no significant difference in the angles formed by the transorbital and supraorbital trajectories targeting the NAc, SCG, and LHA in the sagittal and axial planes between the cadaveric and TGN groups ($p>0.05$).

All trajectory lengths were measured from the dura to target. The lengths of the transorbital and supraorbital trajectories to the NAc, SCG, and LHA (right and left side) were significantly longer in the cadaver group than in the TGN group ($p<0.05$) (Table I).

Furthermore, the transorbital trajectories to the NAc, SCG, and LHA (right and left side) were significantly shorter than the supraorbital trajectories ($p<0.05$) (Table II).

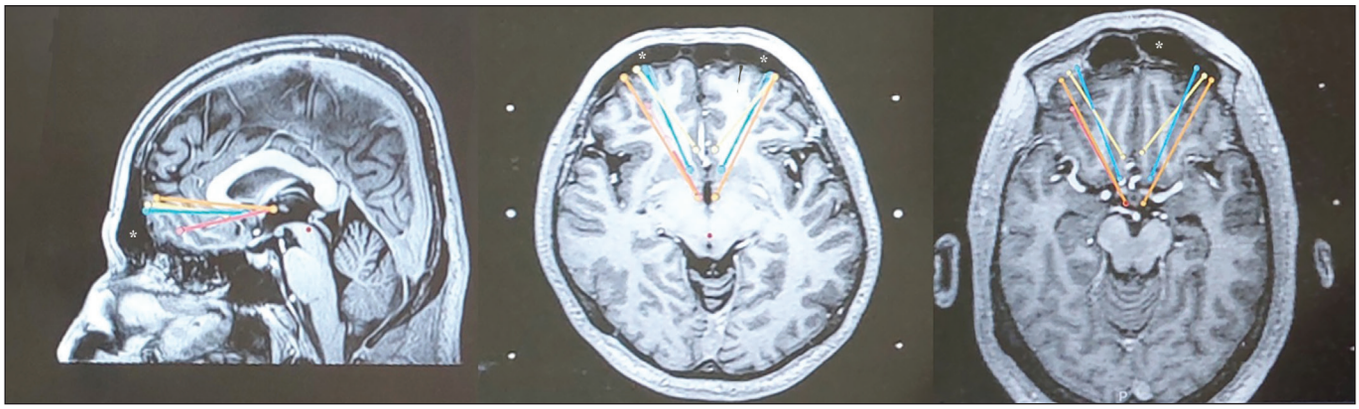

**Figure 13:** Planned supraorbital trajectory passing through the frontal sinus ***.** Frontal Sinus, **Blue line.** Supraorbital Nucleus accumbens trajectory, **Yellow line.** Supraorbital Subcallosal Cingulate gyrus trajectory, **Orange line.** supraorbital trajectory to the lateral hypothalamic area, **Pink line.** Transorbital trajectory to the hypothalamic area.

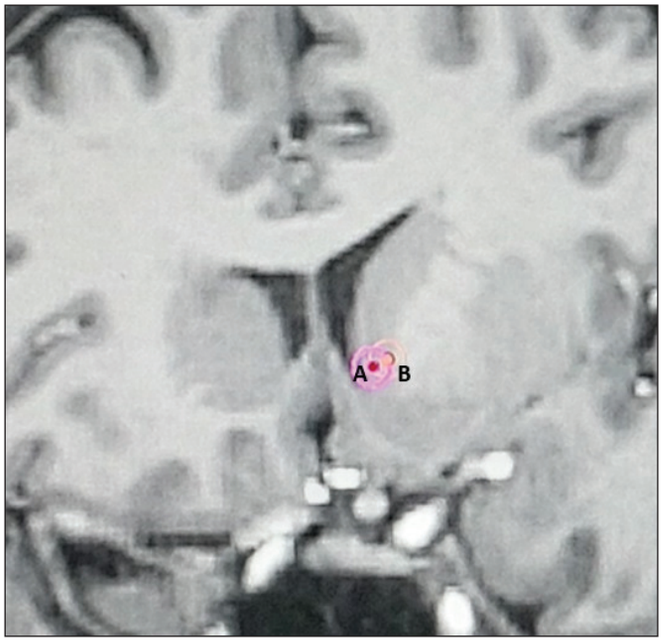


**Figure 14:** Transorbital trajectories to the **A)** nucleus accumbens and **B)** lateral hypothalamic area (Prob's eye view).

There was no significant difference in the lengths of the transorbital and supraorbital trajectories to the NAc, SCG, and LHA between the right and left approaches (Table III).

In the cadavers, there was a significant difference in the lengths of the trajectories to the NAc and SCG between the transorbital/supraorbital approach and the Kocher's approach ($p<0.05$). However, there was no significant difference in the length of the trajectory to the LHA between the supraorbital/transorbital approach and the Kocher's approach ($p>0.05$). Although the trajectory lengths to the NAc and SCG via the supraorbital and transorbital approach was significantly shorter than that via the Kocher's approach, the difference in trajectory length to the LHA via the two approaches was not statistically significant (Table IV).

## DISCUSSION

Psychosurgical approaches introduced by Amaro Fiamberti, Walter Freeman, and James Watts in 1936–37 remained unused for approximately 30 years due to its severe side effects and high risk of complications. However, with the technological developments in the last 15 years, studies on this subject have gained attention because the procedures are more selective and lower-risk. DBS has demonstrated promising results in the treatment of substance addiction, obsessive-compulsive disorder, depression, and aggression (3,4,35). However, the positive outcomes in movement disorder studies and advancements in technology have resulted in stereotactic surgical approaches away from the skull base, with surgical trajectories originating from the coronal suture and its surroundings. Surgical access sites at the level of the coronal suture, which are routinely used in current neurosurgery practice, require long tracts that pass through functional anatomical structures, such as the lateral ventricle, thalamic nuclei, and internal capsule, to achieve psychosurgical stereotactic goals in the anterior and middle fossa. Thus, infarcts and intraventricular hemorrhages can occur in extrapyramidal system structures (8,10). Furthermore, trajectories that pass through the ventricles negatively affect the targeting accuracy (37).

The shell region of the NAc, particularly its caudo-medial and subventricular portions, functions as a limbic-motor interface and plays a role in variable cognitive, emotional, and psychomotor functions in psychopathologies such as obsessive-compulsive disorder and addiction (33,34). Following the reports of successful alcohol deaddiction using DBS therapies targeting the NAc, DBS has demonstrated promising results for the treatment of cocaine and heroin addiction (13,21,27,33,36).

Anatomical studies have demonstrated that the anteroposterior axis of NAc is longer than the dorsal-ventral axis (23). When examining the supraorbital and transorbital trajectories, we found that the entry angles of the electrodes were more parallel to the axial plane of the AC-PC, allowing for a longer path within the NAc and placement of more electrodes

**Table I:** Comparison of Trajectory Lengths Measured from Dura in Cadavers and TGN Cases with Independent t-test and Mann-Whitney-U Test

| Trajectory Lengths | Avg ± SD (mm) | Median (min - max) (mm) | p-value |
|---|---|---|---|
| **Transorbital NAc** | | | |
| Cadaver | 63.31 ± 3.20 | 59.96 (55.28 - 74.98) | 0.001* |
| TGN Cases | 41.99 ± 0.72 | 42.25 (31.60 - 50.40) | |
| **Transorbital SCG** | | | |
| Cadaver | 54.06 ± 1.88 | 53.58 (49.23 - 60.31) | <0.001** |
| TGN Cases | 42.86 ± 7.85 | 35.45 (24.90 - 48.00) | |
| **Transorbital LHA** | | | |
| Cadaver | 77.46 ± 2.43 | 79.15 (69.70 - 83.70) | <0.001* |
| TGN Cases | 54.31 ± 0.75 | 54.40 (42.90 - 65.20) | |
| **Supraorbital NAc** | | | |
| Cadaver | 67.93 ± 2.43 | 66.80 (61.77 - 75.96) | <0.001** |
| TGN Cases | 55.30 ± 0.54 | 55.15 (50.10 - 64.70) | |
| **Supraorbital SCG** | | | |
| Cadaver | 57.87 ± 1.75 | 58.49 (50.35 - 63.00) | <0.001* |
| TGN Cases | 46.79 ± 0.52 | 49.95 (41.60 - 57.60) | |
| **Supraorbital LHA** | | | |
| Cadaver | 81.60 ± 2.65 | 83.43 (71.18 - 89.48) | <0.001* |
| TGN Cases | 67.57 ± 0.64 | 67.75 (59.00 - 75.80) | |

** Independent t test ** Mann-Whitney-U test,* ***Avg:*** *Average,* ***SD:*** *Standard deviation,* ***Min:*** *Minimum,* ***Max:*** *Maximum.*

**Table II:** Comparison of Lengths Between Transorbital and Supraorbital Measurements in All Measurements with Independent t-Test And Mann-Whitney-U Test

| | Mean ± SD (mm) | Median (min - maks) (mm) | p-value |
|---|---|---|---|
| **NAc** | | | |
| transorbital | 44.77 ± 1.30 | 42.85 (31.60-74.98) | <0.001** |
| supraorbital | 56.95 ± 0.84 | 55.80 (50.10-75.96) | |
| **SCG** | | | |
| transorbital | 37.66 ± 7.79 | 36.00 (24.90-60.31) | <0.001** |
| supraorbital | 48.23 ± 0.75 | 47.35 (41.60-63.00) | |
| **LHA** | | | |
| transorbital | 57.33 ± 1.36 | 55.10 (42.90-83.70) | <0.001* |
| supraorbital | 69.40 ± 0.95 | 68.65 (59.00-89.48) | |

** Independent t test ** Mann-Whitney-U test,* ***Avg:*** *Average,* ***SD:*** *Standard deviation,* ***Min:*** *Minimum,* ***Max:*** *Maximum.*

in the area to be stimulated. SCG has critical projections to the ventral striatum, NAc, and limbic cortical circuitry via diffusion tractography, and it is associated with visceromotor and autonomic physiology. Positron emission tomography studies in patients with depression have demonstrated an increased blood flow to this region compared to the normal population, which decreased after treatment with SSRIs (7). Following following the publication of these studies, several patients have benefited from SCG-specific DBS applications for the treatment of treatment-resistant depression (14,30). Despite study findings suggesting that SCG is a promising target for depression treatment and that its stimulation can affect a wide network involved in depression pathology, a multi-center randomized study examining its six-months outcome did not yield the desired therapeutic antidepressant effect (16). Although studies with longer follow-up periods or those targeting the superolateral branch of the medial forebrain bundle using diffusion tensor imaging, rather than indirect SCG coordinates, have reported positive results for depression treatment, a clear treatment protocol has not yet been established

**Table III:** Comparison of Right and Left Length Measurements with Mann-Whitney-U Test

| | Mean ± SD (mm) | Median (min - max) (mm) | p-value |
|---|---|---|---|
| **Transorbital NAc** | | | |
| Left | 44.46 ± 1.79 | 42.30 (31.60 - 71.17) | 0.878** |
| Right | 45.09 ± 1.92 | 43.10 (33.70 - 74.98) | |
| **Transorbital SCG** | | | |
| Left | 37.34 ± 7.41 | 36.10 (24.90 - 56.12) | 0.733** |
| Right | 37.68 ± 1.76 | 35.90 (28.10 - 60.31) | |
| **Transorbital LHA** | | | |
| Left | 57.47 ± 1.84 | 55.00 (46.20 - 79.24) | 0.921** |
| Right | 57.19 ± 2.05 | 55.20 (42.90 - 83.70) | |
| **Supraorbital NAc** | | | |
| Left | 56.72 ± 1.16 | 55.20 (50.50 - 74.19) | 0.709** |
| Right | 57.18 ± 1.24 | 56.10 (50.10 - 75.96) | |
| **Supraorbital SCG** | | | |
| Left | 47.75 ± 1.06 | 47.20 (41.90 - 63.00) | 0.482** |
| Right | 48.71 ± 1.07 | 47.40 (41.60 - 60-42) | |
| **Supraorbital LHA** | | | |
| Left | 68.75 ± 1.39 | 67.80 (59.00 - 89.48) | 0.356** |
| Right | 70.04 ± 1.32 | 69.40 (60.70 - 84.95) | |

** *Mann-Whitney-U test,* ***Avg:*** *Average,* ***SD:*** *Standard deviation,* ***Min:*** *Minimum,* ***Max:*** *Maximum.*

**Table IV:** Comparison of Trajectory Lengths from Kocher's Point, Supraorbital, and Transorbital to NAc, SCG, and LHA Targets in Cadavers with Independent t-test

| | Avg ± SD (mm) | Median (min - max) (mm) | p-value |
|---|---|---|---|
| **NAc** | | | |
| Kocher | 76.94 ± 1.85 | 76.00 (71.78 - 84.05) | 0.004* |
| Transorbital | 63.31 ± 3.20 | 59.96 (55.28 - 74.98) | |
| **SCG** | | | |
| Kocher | 74.83 ± 1.27 | 75.17 (69.35 - 79.09) | <0.001* |
| Transorbital | 54.06 ± 1.88 | 53.58 (49.23 - 60.31) | |
| **LHA** | | | |
| Kocher | 77.46 ± 2.98 | 75.65 (69.87 - 87.94) | 0.999* |
| Transorbital | 77.46 ± 2.43 | 79.15 (69.70 - 83.70) | |
| **NAc** | | | |
| Kocher | 76.94 ± 1.85 | 76.00 (71.78 - 84.05) | 0.015* |
| Supraorbital | 67.93 ± 2.43 | 66.80 (61.77 - 75.96) | |
| **SCG** | | | |
| Kocher | 74.83 ± 1.27 | 75.17 (69.35 - 79.09) | <0.001* |
| Supraorbital | 57.87 ± 1.75 | 58.49 (50.35 - 63.00) | |
| **LHA** | | | |
| Kocher | 77.46 ± 2.98 | 75.65 (69.87 - 87.94) | 0.325* |
| Supraorbital | 81.60 ± 2.65 | 83.43 (71.18 - 89.48) | |

** Independent t test,* ***Avg:*** *Average,* ***SD:*** *Standard deviation,* ***Min:*** *Minimum,* ***Max:*** *Maximum.*

(1,4,24). In studies targeting the SCG via the Kocher's approach, the placement of the electrodes have been debated. Placing the electrodes more anteriorly may affect more fibers of the cingulate bundle. However, placing the electrodes more posteriorly may theoretically affect the projection set that originates and separates from the SCG. This projection set reaches the uncinate fascicle, thalamus, hypothalamus, and brainstem, potentially leading to a stronger antidepressant effect (14,18). However, the greatest challenge in targeting the posterior boundaries of the SCG is surgical safety because the anterior cerebral arteries lie close to that region (14). Reaching this target via a supraorbital or transorbital trajectory enables the use of a safer trajectory that does not target the anterior cerebral arteries and the modulation of this area from anterior to posterior.

Studies targeting hypothalamic regions have reported targeting the posteromedial hypothalamus for the treatment of medication-resistant pain and aggression and targeting the LHA for the treatment of obesity. Although DBS targeting the posteromedial hypothalamus has yielded positive results in the treatment of medication-resistant pain and aggression, and DBS targeting the LHA has demonstrated an increase in metabolism rates in the treatment of intractable obesity, it has not been highly successful in achieving weight loss (11,35).

Additionally, the benefit of projections extending from the orbital frontal cortex to the hypothalamus has been reported in hypothalamic-targeted DBS for the prevention of uncontrollable treatment-resistant aggressive behavior such as intermittent explosive disorder (11). By selecting either the transorbital or supraorbital approach during electrode placement, trajectories within and parallel to these projections can be created, allowing for more targeted stimulation. Stimulation of both the projections extending from the orbital frontal cortex and the hypothalamus by DBS may lead to a more effective response.

The number of stereotactic procedures targeting the hypothalamic region has increased in conjunction with radiofrequency ablation treatments for hypothalamic hamartomas. A systematic review comprising of 388 patients reported a seizure-free rate of 69.2%, despite some patients requiring up to three reoperations (20). Conventional stereotactic approaches are used in radiofrequency thermocoagulation for hypothalamic hamartomas, necessitating the passage of several tracts through the internal capsule and thalamic structures. With each additional tract created during reoperations, the risk of complications also increases (32). This indicates that the use of trajectories passing through non-eloquent areas may reduce the risk of complications.

Our study results indicate that the use of the transorbital approach allows for shorter trajectories compared to the supraorbital approach, despite the transorbital approach requiring more technical knowledge and a multidisciplinary approach.

The transorbital approach may be preferred in individuals with drug or alcohol addictions in addition to eating disorders and treatment-resistant obesity, because the trajectory can target NAc and LHA simultaneously (Figure 14).

Given the interconnecting projections between the SCG, prefrontal cortex, and NAc, transorbital and supraorbital trajectories extending from the prefrontal area, where these projections can also be stimulated, may be preferred (26). This may be particularly relevant for patients with concurrent depression and eating disorders, addiction, or all three conditions. Ultimately, transorbital and supraorbital approaches offers a spectrum of trajectories, with which the underlying neuroanatomy and the specific clinical needs of each patient can be better met.

In our study, the transorbital and supraorbital trajectories to the NAc and SCG were shorter than the trajectory to the LHA via the Kocher's approach (Table IV). Therefore, the supraorbital and transorbital approaches may reduce the risk of complications if the targets are the SCG and NAc. However, the depth of the sulcal structures of the frontal orbital gyrus, which is used as the parenchymal entry point in transorbital approaches, may vary. In some patients, a trans-sulcal approach may be required, which can increase the risk of the trajectory passing through vascular structures and causing an intracranial bleeding. Thus, the anatomy of each patient should be carefully evaluated and the potential risks and benefits of the different DBS trajectories should be considered. Furthermore, because the structure of the frontal sinus varies, the frontal sinus may not be avoidable via the supraorbital approach in every patient, as seen in our study.

Currently, there is no system that can fix the electrodes in place transorbitally or supraorbitally. However, ongoing studies into wireless DBS technology may pave the way for the development of novel surgical procedures that eliminate the need for device fixation (15).

There are some disadvantages of conducting the study in cadavers. Radiological examinations have revealed that the frontal region can undergo significant displacement, especially due to brain shrinkage and loss of CSF. This can be misleading when measuring the trajectory length in the brain parenchyma of cadavers. However, because electrode targeting error due to CSF loss has little effect on the midline structures, we decided to measure the trajectories from the dura (29). The difference in the trajectories lengths (Table I) between the patients with TGN and the cadavers revealed that these lengths are affected by loss of CSF and brain shrinkage. The absence of a significant difference between the angles formed by the trajectories on the right and left side (Table III) suggests that the cadaver brains are symmetrical and that the midline structures do not shift too much in the sagittal and axial planes. Examination of the radiological images obtained after staining and fixing the cadaver brain reveals that the vascular structures of the stained sections were similar to those obtained with CT angiography, enabling planning of the procedure while avoiding vascular structures. This makes the experimental setup more realistic and usable in studies focusing on vascular structures. In future studies, different fixation methods could be planned to establish setups that are more similar to physiological structures. Additionally, increasing the sample size will ensure that statistically significant data can be obtained.

## CONCLUSION

Targeting hypothalamic structures using the proposed entry angles allowed for simultaneous targeting of the NAc. Furthermore, the electrodes should be positioned more accurately in accordance with the anatomical structure of the NAc, and the electrodes should be placed along the projections containing the subcollosal singulate gyrus and LHA that require stimulation. The use of transorbital/supraorbital approaches enables the creation of shorter and safer trajectories to NAc and SCG targets that trajectories via the Kocher's point and its surroundings. Our study findings suggest that transorbital/supraorbital approaches may offer alternate techniques for stimulating different targets in the prefrontal cortex and may serve as an approach for future clinical use.

**Disclosure Statements**

## ACKNOWLEDGEMENT

We would like to thank Emrah Celtikci for his contributions in fixation and staining the cadaver brains.

**Declarations**

**Funding:** This project was supported by Istanbul Medipol University Scientific Research Projects Department (no: 2022/15) as "Defining Minimally Invasive Stereotactic Transorbital Skull Base Approach in Cadaver Heads."

**Availability of data and materials:** All data generated or analyzed during this study are included in the article and its online supplementary materials. Further inquiries can be directed to the corresponding author.

**Disclosure:** The authors have no conflicts of interest to declare.

**AUTHORSHIP CONTRIBUTION**

Study conception and design: BG, MT

Data collection: BG, BT, NEA

Analysis and interpretation of results: NEA, NCO

Draft manuscript preparation: BG, NCO

Critical revision of the article: MT, BUS

All authors (BG, NCO, NEA, BT, BUS, MT) reviewed the results and approved the final version of the manuscript.

## REFERENCES

1. Bewernick BH, Kayser S, Gippert SM, Switala C, Coenen VA, Schlaepfer TE: Deep brain stimulation to the medial forebrain bundle for depression-long-term outcomes and a novel data analysis strategy. Brain Stimul 10:664-671, 2017. https://doi.org/10.1016/j.brs.2017.01.581
2. Brock M, Dietz H: The small frontolateral approach for the microsurgical treatment of intracranial aneurysms. Neurochirurgia 21:185-191, 1978. https://doi.org/10.1055/s-0028-1090343
3. Chen L, Li N, Ge S, Lozano AM, Lee DJ, Yang C, Li L, Bai Q, Lu H, Wang J, Wang X, Li J, Jing J, Su M, Wei L, Wang X, Gao G: Long-term results after deep brain stimulation of nucleus accumbens and the anterior limb of the internal capsule for preventing heroin relapse: An open-label pilot study. Brain Stimul 12:175-183, 2019. https://doi.org/10.1016/j.brs.2018.09.006
4. Crowell AL, Riva-Posse P, Holtzheimer PE, Garlow SJ, Kelley ME, Gross RE, Denison L, Quinn S, Mayberg HS: Long-term outcomes of subcallosal cingulate deep brain stimulation for treatment-resistant depression. Am J Psychiatry 176:949-956, 2019. https://doi.org/10.1176/appi.ajp.2019.18121427
5. Delashaw JB, Tedeschi H, Rhoton AL: Modified supraorbital craniotomy: Technical note. Neurosurgery 30:954-956, 1992. https://doi.org/10.1227/00006123-199206000-00028
6. Di Somma A, Andaluz N, Cavallo LM, Topczewski TE, Frio F, Gerardi RM, Pineda J, Solari D, Enseñat J, Prats-Galino A, Cappabianca P: Endoscopic transorbital route to the petrous apex: A feasibility anatomic study. Acta Neurochir (Wien) 160:707-720, 2018. https://doi.org/10.1007/s00701-017-3448-x
7. Drevets WC, Ongür D, Price JL: Neuroimaging abnormalities in the subgenual prefrontal cortex: Implications for the pathophysiology of familial mood disorders. Mol Psychiatry 3:220-226, 1998. https://doi.org/10.1038/sj.mp.4000370
8. Elias WJ, Sansur CA, Frysinger RC: Sulcal and ventricular trajectories in stereotactic surgery. J Neurosurg 110:201-207, 2009. https://doi.org/10.3171/2008.7.17625
9. Fedorov A, Beichel R, Kalpathy-Cramer J, Finet J, Fillion-Robin JC, Pujol S, Bauer C, Jennings D, Fennessy F, Sonka M, Buatti J, Aylward S, Miller JV, Pieper S, Kikinis R: 3D Slicer as an image computing platform for the Quantitative Imaging Network. Magn Reson Imaging 30:1323-1341, 2012. https://doi.org/10.1016/j.mri.2012.05.001
10. Fenoy AJ, Simpson RK: Risks of common complications in deep brain stimulation surgery: Management and avoidance. J Neurosurg 120:132-139, 2014. https://doi.org/10.3171/2013.10.JNS131225
11. Franzini A, Messina G, Cordella R, Marras C, Broggi G: Deep brain stimulation of the posteromedial hypothalamus: Indications, long-term results, and neurophysiological considerations. Neurosurg Focus 29:E13, 2010. https://doi.org/10.3171/2010.5.FOCUS1094
12. Gazzeri R, Nishiyama Y, Ph.D, Teo C: Endoscopic supraorbital eyebrow approach for the surgical treatment of extraaxialand intraaxial tumors. Neurosurgical Focus 37:E20, 2014. https://doi.org/10.3171/2014.7.FOCUS14203
13. Gonçalves-Ferreira A, do Couto FS, Rainha Campos A, Lucas Neto LP, Gonçalves-Ferreira D, Teixeira J: Deep brain stimulation for refractory cocaine dependence. Biol Psychiatry 79:e87-89, 2016. https://doi.org/10.1016/j.biopsych.2015.06.023
14. Hamani C, Mayberg H, Snyder B, Giacobbe P, Kennedy S, Lozano AM: Deep brain stimulation of the subcallosal cingulate gyrus for depression: Anatomical location of active contacts in clinical responders and a suggested guideline for targeting. J Neurosurg 111:1209-1215, 2009. https://doi.org/10.3171/2008.10.JNS08763
15. Hescham SA, Chiang PH, Gregurec D, Moon J, Christiansen MG, Jahanshahi A, Liu H, Rosenfeld D, Pralle A, Anikeeva P, Temel Y: Magnetothermal nanoparticle technology alleviates parkinsonian-like symptoms in mice. Nat Commun 12:5569, 2021. https://doi.org/10.1038/s41467-021-25837-4

16. Holtzheimer PE, Husain MM, Lisanby SH, Taylor SF, Whitworth LA, McClintock S, Slavin KV, Berman J, McKhann GM, Patil PG, Rittberg BR, Abosch A, Pandurangi AK, Holloway KL, Lam RW, Honey CR, Neimat JS, Henderson JM, DeBattista C, Rothschild AJ, Pilitsis JG, Espinoza RT, Petrides G, Mogilner AY, Matthews K, Peichel D, Gross RE, Hamani C, Lozano AM, Mayberg HS: Subcallosal cingulate deep brain stimulation for treatment-resistant depression: A multisite, randomised, sham-controlled trial. Lancet Psychiatry 4:839-849, 2017. https://doi.org/10.1016/S2215-0366(17)30371-1
17. Jane JA, Park TS, Pobereskin LH, Winn HR, Butler AB: The supraorbital approach: Technical note. Neurosurgery 11:537-542, 1982. https://doi.org/10.1227/00006123-198210000-00016
18. Johansen-Berg H, Gutman DA, Behrens TEJ, Matthews PM, Rushworth MFS, Katz E, Lozano AM, Mayberg HS: Anatomical connectivity of the subgenual cingulate region targeted with deep brain stimulation for treatment-resistant depression. Cereb Cortex 18:1374-1383, 2008. https://doi.org/10.1093/cercor/bhm167
19. Kassam AB, Gardner P, Snyderman C, Mintz A, Carrau R: Expanded endonasal approach: Fully endoscopic, completely transnasal approach to the middle third of the clivus, petrous bone, middle cranial fossa, and infratemporal fossa. Neurosurg Focus 19:E6, 2005. https://doi.org/10.3171/foc.2005.19.1.7
20. Kondajji AM, Evans A, Lum M, Kulinich D, Unterberger A, Ding K, Duong C, Patel K, Yang I: A systematic review of stereotactic radiofrequency ablation for hypothalamic hamartomas. J Neurolog Sci 424:117428, 2021. https://doi.org/10.1016/j.jns.2021.117428
21. Kuhn J, Lenartz D, Huff W, Lee S, Koulousakis A, Klosterkoetter J, Sturm V: Remission of alcohol dependency following deep brain stimulation of the nucleus accumbens: Valuable therapeutic implications? J Neurol Neurosurg Psychiatry 78:1152-1153, 2007. https://doi.org/10.1136/jnnp.2006.113092
22. Mai JK, Majtanik M, Paxinos G: Atlas of the Human Brain. San Diego: Academic Press, 2015
23. Mavridis I, Boviatsis E, Anagnostopoulou S: Anatomy of the human nucleus accumbens: A combined morphometric study. Surg Radiol Anat 33:405-414, 2011. https://doi.org/10.1007/s00276-010-0766-6
24. Merkl A, Aust S, Schneider GH, Visser-Vandewalle V, Horn A, Kühn AA, Kuhn J, Bajbouj M: Deep brain stimulation of the subcallosal cingulate gyrus in patients with treatment-resistant depression: A double-blinded randomized controlled study and long-term follow-up in eight patients. J Affect Disord 227:521-529, 2018. https://doi.org/10.1016/j.jad.2017.11.024
25. Moe KS, Bergeron CM, Ellenbogen RG: Transorbital neuroendoscopic surgery. Neurosurgery 67:ons16-28, 2010. https://doi.org/10.1227/01.NEU.0000373431.08464.43
26. Morishita T, Fayad SM, Higuchi M aki, Nestor KA, Foote KD: Deep brain stimulation for treatment-resistant depression: Systematic review of clinical outcomes. Neurotherapeutics 11:475-484, 2014. https://doi.org/10.1007/s13311-014-0282-1
27. Müller UJ, Sturm V, Voges J, Heinze HJ, Galazky I, Heldmann M, Scheich H, Bogerts B: Successful treatment of chronic resistant alcoholism by deep brain stimulation of nucleus accumbens: First experience with three cases. Pharmacopsychiatry 42:288-291, 2009. https://doi.org/10.1055/s-0029-1233489
28. Neto LL, Oliveira E, Correia F, Ferreira AG: The human nucleus accumbens: where is it? A stereotactic, anatomical and magnetic resonance imaging study. Neuromodulation 11:13-22, 2008. https://doi.org/10.1111/j.1525-1403.2007.00138.x
29. Petersen EA, Holl EM, Martinez-Torres I, Foltynie T, Limousin P, Hariz MI, Zrinzo L: Minimizing brain shift in stereotactic functional neurosurgery. Operat Neurosurg 67:ons213, 2010. https://doi.org/10.1227/01.NEU.0000380991.23444.08
30. Puigdemont D, Portella M, Pérez-Egea R, Molet J, Gironell A, de Diego-Adeliño J, Martín A, Rodríguez R, Àlvarez E, Artigas F, Pérez V: A randomized double-blind crossover trial of deep brain stimulation of the subcallosal cingulate gyrus in patients with treatment-resistant depression: A pilot study of relapse prevention. J Psychiatry Neurosci 40:224-231, 2015. https://doi.org/10.1503/jpn.130295
31. Sanan A, Aziz KMA, Janjua RM, van Loveren HR, Keller JT: Colored silicone injection for use in neurosurgical dissections: Anatomic technical note. Neurosurgery 45:1267, 1999. https://doi.org/10.1097/00006123-199911000-00058
32. Shirozu H, Masuda H, Kameyama S: Repeat stereotactic radiofrequency thermocoagulation in patients with hypothalamic hamartoma and seizure recurrence. Epilepsia Open 5:107-120, 2020. https://doi.org/10.1002/epi4.12378
33. Sturm V, Lenartz D, Koulousakis A, Treuer H, Herholz K, Klein JC, Klosterkötter J: The nucleus accumbens: A target for deep brain stimulation in obsessive-compulsive- and anxiety-disorders. J Chem Neuroanat 26:293-299, 2003. https://doi.org/10.1016/j.jchemneu.2003.09.003
34. Voges J, Müller U, Bogerts B, Münte T, Heinze HJ: Deep brain stimulation surgery for alcohol addiction. World Neurosurg 80:S28.e21-31, 2013. https://doi.org/10.1016/j.wneu.2012.07.011
35. Whiting DM, Tomycz ND, Bailes J, De Jonge L, Lecoultre V, Wilent B, Alcindor D, Prostko ER, Cheng BC, Angle C, Cantella D, Whiting BB, Mizes JS, Finnis KW, Ravussin E, Oh MY: Lateral hypothalamic area deep brain stimulation for refractory obesity: A pilot study with preliminary data on safety, body weight, and energy metabolism. J Neurosurg 119:56-63, 2013. https://doi.org/10.3171/2013.2.JNS12903
36. Zhou H, Xu J, Jiang J: Deep brain stimulation of nucleus accumbens on heroin-seeking behaviors: A case report. Biol Psychiatry 69:e41-42, 2011. https://doi.org/10.1016/j.biopsych.2011.02.012
37. Zrinzo L, Hulzen ALJ van, Gorgulho AA, Limousin P, Staal MJ, Salles AAFD, Hariz MI: Avoiding the ventricle: A simple step to improve accuracy of anatomical targeting during deep brain stimulation: Clinical article. J Neurosurg 110:1283-1290, 2009. https://doi.org/10.3171/2008.12.JNS08885

Lengths of Trajectories Measured from Dura to Targets in Cadavers

| Trajectory lenght | Cadaver 1 | | Cadaver 2 | | Cadaver 3 | |
|---|---|---|---|---|---|---|
| | Right | Left | Right | Left | Right | Left |
| **Transorbital - NAc (mm)** | 58.53 | 60.56 | 59.37 | 55.28 | 74.98 | 71.17 |
| **Transorbital - SCG (mm)** | 49.95 | 49.23 | 57.73 | 51.05 | 60.31 | 56.12 |
| **Transorbital - LHA (mm)** | 69.70 | 70.55 | 82.54 | 79.24 | 83.70 | 79.07 |
| **Supraorbital - NAc (mm)** | 67.02 | 62.10 | 61.77 | 66.59 | 75.96 | 74.19 |
| **Supraorbital - SCG (mm)** | 56.47 | 50.35 | 59 | 63 | 60.42 | 57.99 |
| **Supraorbital - LHA (mm)** | 77.13 | 71.18 | 84.60 | 89.48 | 84.95 | 82.26 |
| **Kocher - NAc (mm)** | 73.55 | 76.93 | 71.78 | 75.07 | 84.05 | 80.28 |
| **Kocher - SCG (mm)** | 69.35 | 75.05 | 75.45 | 79.09 | 75.29 | 74.75 |
| **Kocher - LHA (mm)** | 71.14 | 69.87 | 74.48 | 76.83 | 87.94 | 84.54 |

Lengths of Trajectories Measured from Dura to Targets in TGN Cases

| TGN Cases | Transorbital -NAc (mm) | | Trans orbital-SCG (mm) | | Transorbital -LHA (mm) | | Suprasorbital-NAc (mm) | | Supraorbital - SCG (mm) | | Supraorbital - LHA (mm) | |
|---|---|---|---|---|---|---|---|---|---|---|---|---|
| | Right | Left | Right | Left | Right | Left | Right | Left | Right | Left | Right | Left |
| 1 | 38.3 | 42.9 | 35 | 36.8 | 53 | 54.9 | 52 | 55 | 47.3 | 50 | 74.7 | 68.8 |
| 2 | 42.2 | 39.5 | 34.3 | 32.5 | 52.8 | 50.4 | 59.6 | 56.2 | 49.4 | 47.5 | 70.1 | 67.4 |
| 3 | 45.7 | 42.3 | 36.4 | 33.3 | 55.2 | 53.9 | 57.3 | 57.3 | 51 | 46.7 | 71 | 68.5 |
| 4 | 36.4 | 42 | 28.1 | 28.1 | 48.8 | 48.8 | 50.5 | 50.5 | 41.6 | 41.9 | 63.6 | 62.2 |
| 5 | 36.3 | 31.6 | 28.8 | 24.9 | 50.7 | 46.2 | 58.9 | 58.4 | 49.6 | 45.3 | 71.1 | 71.4 |
| 6 | 33.7 | 34.6 | 28.6 | 28 | 50.6 | 56.6 | 50.1 | 50.5 | 42.5 | 43.6 | 60.8 | 64.1 |
| 7 | 50.4 | 46.6 | 41.7 | 42.2 | 56.4 | 65.2 | 64.7 | 64.7 | 57.6 | 54.1 | 75.8 | 75.8 |
| 8 | 42.8 | 40.2 | 35.9 | 36.1 | 55.9 | 54.4 | 52 | 55.1 | 45.7 | 49.3 | 65.4 | 69.6 |
| 9 | 40.8 | 38 | 37.1 | 31.4 | 42.9 | 49.3 | 51.5 | 50.8 | 45.2 | 45.3 | 60.7 | 59 |
| 10 | 43.6 | 40.8 | 39.7 | 36.2 | 57.7 | 52.8 | 55.5 | 55.5 | 46.2 | 47.4 | 66 | 66 |
| 11 | 43.1 | 41.5 | 35.9 | 35.9 | 56.6 | 55.5 | 53.2 | 55.2 | 44.1 | 48.3 | 68.3 | 69.1 |
| 12 | 44 | 34.6 | 34.2 | 34.2 | 51.9 | 55.5 | 57.6 | 53.8 | 47.7 | 42.3 | 70.9 | 67.8 |
| 13 | 48.6 | 45.8 | 40 | 348 | 62.1 | 55 | 57.8 | 58 | 43.9 | 43.9 | 64.5 | 64.5 |
| 14 | 47.8 | 47.8 | 39.7 | 39.7 | 60.7 | 60.7 | 58.8 | 53.5 | 48.8 | 42.3 | 72.2 | 63.3 |
| 15 | 41.7 | 42.3 | 34.4 | 39.9 | 54.4 | 56.3 | 56.1 | 56.1 | 46.2 | 46.2 | 69.4 | 66.9 |
| 16 | 36.7 | 41 | 29.9 | 34.4 | 49.6 | 49.6 | 54.5 | 53.7 | 48.7 | 47.9 | 67.7 | 67.7 |
| 17 | 37.8 | 45.9 | 29.3 | 36.3 | 57.4 | 64.5 | 54.1 | 54.1 | 44.2 | 44.2 | 72.1 | 72.1 |
| 18 | 45.6 | 45.6 | 34.2 | 34.2 | 53.5 | 53.5 | 56.1 | 53.2 | 47.4 | 43.4 | 67 | 61.1 |
| 19 | 49 | 49 | 42.5 | 43.6 | 61 | 58 | 57.7 | 57.7 | 50.3 | 50.3 | 68.9 | 68.9 |
| 20 | 39.7 | 43.6 | 33.1 | 40.1 | 48.4 | 51.9 | 52.5 | 52.5 | 47.2 | 47.2 | 64.1 | 64.3 |

*Comparison of the angles made by the trajectories with the axial plane using independent t-test and Mann-Whitney U-test*

Angles Made by Trajectories with the Sagittal and the Axial Plane in Cadavers

| Cadaver | Transorbital - NAc | | | | Transorbital - SCG | | | | Transorbital - LHA | | | | Suprasorbital - NAc | | | | Supraorbital - SCG | | | | Supraorbital - LHA | | | |
|---|---|---|---|---|---|---|---|---|---|---|---|---|---|---|---|---|---|---|---|---|---|---|---|---|
| | Right | | Left | | Right | | Left | | Right | | Left | | Right | | Left | | Right | | Left | | Right | | Left | |
| | Sag | Ax | Sag | Ax | Sag | Ax | Sag | Ax | Sag | Ax | Sag | Ax | Sag | Ax | Sag | Ax | Sag | Ax | Sag | Ax | Sag | Ax | Sag | Ax |
| 1 | 129.3 | 5.4 | 125.8 | 2.6 | 130.3 | 0.7 | 127.2 | 6.1 | 120.2 | 5.7 | 126.2 | 2.8 | 109.9 | 11.6 | 110 | 10.7 | 120.7 | 11.2 | 109.7 | 9.2 | 110.5 | 11.1 | 150.5 | 13.1 |
| 2 | 112.2 | 11.4 | 115.3 | 7.5 | 107.6 | 13.2 | 108.1 | 13.5 | 128.6 | 13.7 | 110.4 | 15.4 | 89.5 | 1.4 | 75.6 | 5 | 83 | 3.9 | 78.8 | 4.7 | 92.2 | 4.7 | 102 | 2.6 |
| 3 | 103.2 | 10.2 | 106.6 | 11.5 | 101.7 | 14.7 | 107.3 | 10.4 | 104.9 | 11.0 | 119 | 17 | 96 | 3.1 | 84.5 | 4.9 | 77.5 | 12.4 | 80.6 | 9.4 | 97 | 3.1 | 90 | 0.1 |

***Sag:*** *Angles made by trajectories with the sagittal plane,* ***Ax:*** *Angles made by trajectories with the axial plane.*

Angles Made by Trajectories with the Sagittal and the Axial Plane in TGN Cases

| TGN Cases | Transorbital - NAc | | | | Transorbital - SCG | | | | Transorbital - LHA | | | | Suprasorbital - NAc | | | | Supraorbital - SCG | | | | Supraorbital - LHA | | | |
|---|---|---|---|---|---|---|---|---|---|---|---|---|---|---|---|---|---|---|---|---|---|---|---|---|
| | Right | | Left | | Right | | Left | | Right | | Left | | Right | | Left | | Right | | Left | | Right | | Left | |
| | Sag | Ax | Sag | Ax | Sag | Ax | Sag | Ax | Sag | Ax | Sag | Ax | Sag | Ax | Sag | Ax | Sag | Ax | Sag | Ax | Sag | Ax | Sag | Ax |
| 1 | 109.6 | 9.9 | 90.6 | 0.3 | 79 | 11.8 | 76.8 | 17.2 | 107.9 | 7.7 | 89.3 | 0.3 | 49.6 | 24.8 | 57.2 | 23.4 | 58.9 | 28.3 | 46.7 | 38.7 | 64.6 | 12.1 | 66.4 | 16.2 |
| 2 | 95 | 3 | 100.5 | 9.3 | 99.9 | 9.9 | 100.3 | 15.7 | 97.6 | 3.9 | 99.3 | 6.9 | 62.5 | 11.4 | 75 | 10.1 | 69.6 | 11.6 | 75.6 | 13.3 | 67.5 | 8.5 | 76.8 | 8.1 |
| 3 | 102.6 | 10.7 | 111.8 | 11.7 | 101.4 | 11.9 | 113.8 | 19.5 | 113.4 | 11.5 | 128.5 | 15.4 | 86.4 | 1.3 | 86.4 | 1.3 | 82 | 5.4 | 89.9 | 0 | 91.8 | 0.7 | 104.5 | 4.1 |
| 4 | 123.6 | 21.2 | 125.1 | 18 | 116.2 | 28.1 | 116.2 | 28.1 | 117.3 | 13.8 | 117.3 | 13.8 | 93.6 | 2 | 93.6 | 2 | 89 | 0.8 | 91.6 | 1.6 | 91.1 | 0.5 | 106.7 | 7.3 |
| 5 | 102.3 | 6.4 | 116.7 | 13.9 | 108.7 | 18.2 | 120.7 | 23.2 | 111.3 | 9.4 | 123.1 | 14.6 | 66.8 | 11.6 | 65.9 | 12.2 | 74.5 | 10.9 | 84.5 | 3.4 | 95.7 | 2.7 | 76.8 | 6.3 |
| 6 | 133.9 | 23.3 | 126.9 | 21 | 107.8 | 21 | 105.6 | 16.7 | 122.8 | 28.4 | 119.9 | 16.6 | 108.2 | 8.8 | 94.7 | 2 | 86.4 | 2.6 | 78.9 | 7.6 | 121 | 11.1 | 100.4 | 5.8 |
| 7 | 109 | 12.8 | 110.9 | 15.5 | 99.3 | 8.1 | 116.3 | 11.1 | 124.8 | 16.8 | 134.4 | 15.4 | 100.6 | 4.5 | 100.6 | 4.5 | 86.1 | 2.6 | 77.2 | 5.6 | 101.3 | 4.8 | 101.3 | 4.8 |
| 8 | 114.4 | 16.6 | 120 | 25 | 108.7 | 28.3 | 111 | 28.4 | 117.5 | 14.9 | 122.8 | 19.9 | 101.9 | 6.3 | 101.4 | 5.1 | 88.2 | 1.5 | 89.8 | 0.1 | 98.9 | 4.5 | 92.6 | 1.6 |
| 9 | 109.7 | 15.6 | 128.6 | 16.1 | 99.7 | 10.3 | 11.6 | 14.2 | 139.4 | 19.3 | 139.7 | 17.6 | 81.3 | 5.4 | 82.5 | 2.9 | 60.2 | 15.1 | 64.2 | 14.3 | 90.1 | 0 | 102.6 | 5.2 |
| 10 | 121.3 | 20.7 | 117 | 19 | 115.1 | 31.5 | 114.9 | 31.3 | 122.2 | 19.5 | 121.4 | 19.3 | 103.4 | 5.4 | 103.4 | 5.4 | 104.5 | 11.5 | 106.9 | 11.1 | 111.1 | 11.6 | 111.1 | 11.6 |
| 11 | 108.4 | 11.3 | 108.1 | 11.7 | 110 | 23 | 110 | 23 | 118.7 | 13.5 | 118.4 | 13.7 | 84.5 | 2.8 | 87.2 | 1.5 | 93.9 | 3 | 77.1 | 8.8 | 77.8 | 4.2 | 89.7 | 0.1 |
| 12 | 108.2 | 12.4 | 108.3 | 11.5 | 104.3 | 12.2 | 104.3 | 12.2 | 122.6 | 16.7 | 112.4 | 16.4 | 87.5 | 1.2 | 75.5 | 7.1 | 84 | 3.5 | 82.8 | 2.7 | 96.2 | 2.7 | 97 | 3.6 |
| 13 | 107.4 | 14.2 | 116.6 | 12.4 | 100.7 | 11.7 | 104.3 | 11.4 | 107.9 | 11.2 | 122 | 14 | 95 | 2.9 | 86.5 | 1.9 | 78.6 | 10.4 | 78.6 | 10.4 | 92 | 1.1 | 92 | 1.1 |
| 14 | 110.9 | 12.6 | 110.9 | 12.6 | 108.4 | 13.9 | 104.8 | 13.9 | 110.6 | 10.6 | 110.6 | 10.6 | 92.1 | 0.7 | 89.1 | 0.5 | 86.4 | 1.7 | 94.1 | 4.2 | 94.6 | 1.4 | 92.4 | 1.2 |
| 15 | 106.7 | 8.9 | 101.7 | 10.7 | 106.2 | 15.3 | 101.1 | 16.5 | 124.3 | 15.8 | 124.3 | 15.8 | 80.7 | 3 | 80.7 | 3 | 90.6 | 0.3 | 90.6 | 0.3 | 102.8 | 7.3 | 102.9 | 5.7 |
| 16 | 128.7 | 26.0 | 125.2 | 19.6 | 109.8 | 25.5 | 102.7 | 11.7 | 129.8 | 22.4 | 129.8 | 22.4 | 129.8 | 22.4 | 129.8 | 22.4 | 78.5 | 7.6 | 86.4 | 4.2 | 111.9 | 9.5 | 111.9 | 9.5 |
| 17 | 139.4 | 37.4 | 124 | 24.8 | 133.2 | 49.9 | 123.2 | 28.4 | 149.2 | 39.9 | 138.1 | 31.3 | 117.1 | 15.9 | 117.1 | 15.9 | 110.8 | 16.5 | 110.8 | 16.5 | 133.5 | 24.1 | 133.5 | 24.1 |
| 18 | 96.2 | 3.2 | 96.2 | 3.2 | 94.1 | 4 | 94.1 | 4 | 103.1 | 5.4 | 103.1 | 5.4 | 68.3 | 9.8 | 77.2 | 5.9 | 68.5 | 12.7 | 77.5 | 9.6 | 82.3 | 2.6 | 88 | 0.7 |
| 19 | 91.6 | 1.1 | 91.6 | 1.1 | 88.6 | 1.4 | 92.1 | 2.4 | 96.5 | 4.3 | 91.4 | 0.6 | 77.9 | 7.5 | 77.9 | 7.5 | 71.8 | 15.8 | 71.8 | 15.8 | 73.3 | 8.1 | 73.3 | 8.1 |
| 20 | 101 | 5.7 | 84.8 | 2.3 | 102.7 | 10.6 | 91.4 | 1.3 | 101.6 | 4.5 | 91.3 | 0.5 | 77 | 7 | 77 | 7 | 80.2 | 8.6 | 80.2 | 8.6 | 74.4 | 7.6 | 69.5 | 10.2 |

***Sag:*** *Angles made by trajectories with the sagittal plane,* ***Ax:*** *Angles made by trajectories with the axial plane*

| Angles of trajectories with axial plane | Avg ± SD | Median (Min - Max) | p-value |
|---|---|---|---|
| **Transorbital NAc** | | | |
| Cadaver | 8.10 ± 1.46 | 8.85 (2.60 - 11.50) | 0.125* |
| TGN Cases | 13.31 ± 1.26 | 12.50 (0.3 - 37.40) | |
| **Transorbital SCG** | | | |
| Cadaver | 9.76 ± 2.20 | 11.80 (0.70 - 14.70) | 0.087** |
| TGN Cases | 16.92 ± 1.57 | 14.75 (1.30 - 49.9) | |
| **Transorbital LHA** | | | |
| Cadaver | 10.93 ± 2.29 | 12.35 (2.80 - 17.00) | 0.397** |
| TGN Cases | 14.00 ±1.29 | 14.30 (0.3 - 39.9) | |
| **Supraorbital NAc** | | | |
| Cadaver | 6.11 ± 1.68 | 4.95 (1.40 - 11.60) | 0.937** |
| TGN Cases | 7.40 ± 1.05 | 5.40 (0.50 - 24.80) | |
| **Supraorbital SCG** | | | |
| Cadaver | 8.46 ± 1.40 | 9.30 (3.90 - 12.40) | 0.667** |
| TGN Cases | 8.68 ± 1.24 | 8.10 (0.00 - 38.70) | |
| **Supraorbital LHA** | | | |
| Cadaver | 5.78 ± 2.10 | 3.90 (0.10 - 13.10) | 0.812** |
| TGN Cases | 6.51 ± 0.89 | 5.45 (0.00 - 24.10) | |

**Independent t test ** Mann-Whitney-U test,* ***Avg:*** *Average,* ***SD:*** *Standard deviation,* ***Min:*** *Minimum,* ***Max:*** *Maximum.*

Comparison of Angles Made by Trajectories with the Axial Plane Using Independent t-test and Mann-Whitney U Test

| Angles of trajectories with the sagittal plane | Avg ± SD | Median (Min - Max) | p-value |
|---|---|---|---|
| **Transorbital NAc** | | | |
| Cadaver | 115.40 ± 4.23 | 113.75 (103.20 - 129.30) | 0.412* |
| TGN Cases | 110.88 ± 2.00 | 109.65 (84.80 - 139.40) | |
| **Transorbital SCG** | | | |
| Cadaver | 113.70±4.86 | 107.85 (101.70-130.30) | 0.170** |
| TGN Cases | 102.72±2.90 | 104.55 (11.60-133.20) | |
| **Transorbital LHA** | | | |
| Cadaver | 118.21 ± 3.71 | 119.60 (104.90 - 128.60) | 0.825* |
| TGN Cases | 116.89 ± 2.23 | 199.498 (89.30 - 149.20) | |
| **Supraorbital NAc** | | | |
| Cadaver | 94.25 ± 5.66 | 92.75 (75.60 - 110.00) | 0.423* |
| TGN Cases | 88.07 ± 2.82 | 86.43 (49.60 - 129.80) | |
| **Supraorbital SCG** | | | |
| Cadaver | 91.76 ± 7.59 | 81.80 (77.50 - 120.70) | 0.397** |
| TGN Cases | 82.44 ± 2.10 | 82.40 (46.70 - 110.80) | |
| **Supraorbital LHA** | | | |
| Cadaver | 107.03 ± 9.19 | 99.50 (90.00 - 150.50) | 0.245** |
| TGN Cases | 94.03 ± 2.65 | 93.60 (64.60 - 133.50) | |

**Independent t test ** Mann-Whitney-U test,* ***Avg:*** *Average,* ***SD:*** *Standard deviation,* ***Min:*** *Minimum,* ***Max:*** *Maximum.*